

Super-stable parallel flows of multiple visco-plastic fluids

I.A. Frigaard

*Department of Mathematics and Department of Mechanical Engineering, University of British Columbia,
2324 Main Mall, Vancouver, BC, Canada V6T 1Z4*

Received 14 August 2000; received in revised form 5 June 2001

Abstract

We consider the stability of a multi-layer plane Poiseuille flow of two Bingham fluids. It is shown that this two-fluid flow is frequently more stable than the equivalent flow of either fluid alone. This phenomenon of *super-stability* results only when the yield stress of the fluid next to the channel wall is larger than that of the fluid in the centre of the channel, which need not have a yield stress. Our result is in direct contrast to the stability of analogous flows of purely viscous generalised Newtonian fluids, for which short wavelength interfacial instabilities can be found at relatively low Reynolds numbers. The results imply the existence of parameter regimes where *visco-plastic lubrication* is possible, permitting transport of an inelastic generalised Newtonian fluid in the centre of a channel, lubricated at the walls by a visco-plastic fluid, travelling in a stable laminar flow at higher flow rates than would be possible for the single fluid alone. © 2001 Elsevier Science B.V. All rights reserved.

Keywords: Bingham fluid; Stability; Orr–Sommerfeld equation; Lubrication; Multi-layer flow

1. Introduction

The importance of maintaining stable interfaces in multi-layer duct flows relates largely to the prevalence of these flows in various extrusion and transport processes. In one group of applications, the fluid which contacts the walls of the duct is used to lubricate the passage of the other, i.e. increase throughput and/or isolate the extruded fluid from contact with the wall. In another group of applications, the lubricating fluid may form part of a co-extruded product, e.g. a multi-layer sheet. Common to both groups of applications is the need to avoid instabilities at the interface between the fluids. These instabilities and their onset often severely limit rates of production/transport. In this paper, we show that use of a visco-plastic (Bingham) fluid in place of a purely viscous lubricating fluid can eliminate linear interfacial instabilities. We believe there is a consequent potential for application in processes of the type described.

The earliest theoretical investigations of instability due to viscosity stratification is probably the classical study of Yih [1]. Subsequent authors have considered various aspects of this problem for multi-layer Couette, Poiseuille and Couette–Poiseuille flows of Newtonian fluids, e.g. [2–4], and a fairly extensive review of this literature is given in [5]. Broadly speaking, the linear stability of immiscible iso-density

flows requires a sufficiently large surface tension and that the lubricating fluid be less viscous. The latter tends to stabilise long wavelength instabilities, whereas without interfacial tension short wavelength instabilities occur at the interface. Instabilities originate at the interface and occur at Reynolds numbers that are far below those for which the flows of either fluid alone would become unstable. Suggested explanations of physical mechanisms that govern this type of instability have been given in [6,7].

A number of authors have considered the stability of multi-layer flows of non-Newtonian fluids. In this paper, we are interested mostly in plane Poiseuille flows of inelastic non-Newtonian fluids. Therefore, we do not review the large literature on multi-layer visco-elastic flows. Linear stability of multi-layer Couette and Poiseuille flows of power law fluids have been treated extensively in [8–11], both by developing the analogous analytic expressions to the Newtonian fluid problems, and by numerical solution of the linear stability problems. Pinarbasi and Liakopoulos [12] have considered the stability of a two-layer Poiseuille flow of both Carreau–Yasuda and Bingham-like fluids. With reference to [10–12], we note that the two-layer Poiseuille flows considered are different to the Poiseuille flows that we consider later. Also confusing from the point of view of this paper, is that Pinarbasi and Liakopoulos do not model a true Bingham fluid (i.e. with a yield stress). Instead, they choose a form of regularised viscosity model in which the effective viscosity attains a Newtonian limit at zero shear-rate. This modified constitutive model is then qualitatively similar to the Carreau–Yasuda model that is also studied in [12].

The results of [8–12] are qualitatively similar to those found for the corresponding Newtonian fluid flows. Interfacial instabilities again arise at moderate Reynolds numbers. Although the non-Newtonian rheology can positively influence the stability, it is not effective in wholly eliminating interfacial instabilities. If the physical mechanism of instability described in [6] is accepted, then sufficiently close to the fluid–fluid interface, the non-Newtonian character of these fluids is simply not recognised (i.e. the dominant feature at the interface is a discontinuity in a finite constant viscosity between the two fluids), and we should therefore expect similar behaviour with respect to the short wavelength instabilities as for two Newtonian fluids. On the other hand, the expressions for long wavelength instability can be derived by using regular perturbation methods, from the linearised stability equations for each generalised Newtonian fluid (e.g. as in [10]). The methodology is analogous to that used in the Newtonian fluid studies and hence the qualitative similarity is not surprising.

In this paper, we address the stability problem for a plane Poiseuille flow of two Bingham fluids. Our basic flow configuration is a three-layer flow, with a central layer of fluid 1 being lubricated by two layers of fluid 2 at the walls, see Fig. 1a. The aim of the paper is to demonstrate that, when a true visco-plastic is used as the lubricating fluid, linear interfacial instabilities occurring between the 2 fluid layers, can be wholly eliminated. Instead, the flow becomes linearly unstable only through the same shear instability mechanisms as for the flow of a single Bingham fluid. Since shear instabilities typically occur in long ducts at Reynolds numbers of order 10^3 , whereas interfacial instabilities in multi-layer flows without yield stress fluids are typically of order 1–10 in analogous flows, e.g. [2–4,8–12], the gain in stability is considerable. The general area for application of our results is to use a mobile visco-plastic fluid layer to lubricate the passage of another fluid.

A situation in which multi-layer flows of the type described can occur is in the cementing of an oil well in a laminar flow regime. Here, one shear-thinning visco-plastic fluid is displaced by another, along a narrow annulus. It is important that the in-situ fluid, the drilling mud, is completely displaced by the displacing fluid, a spacer fluid or cement slurry. Ignoring azimuthal flows in the annulus leads to a two-dimensional displacement flow involving two visco-plastic fluids, which has been recently studied in [13,14]. These two studies focus on the case in which the displacing fluid fingers through the displaced fluid, allowing a

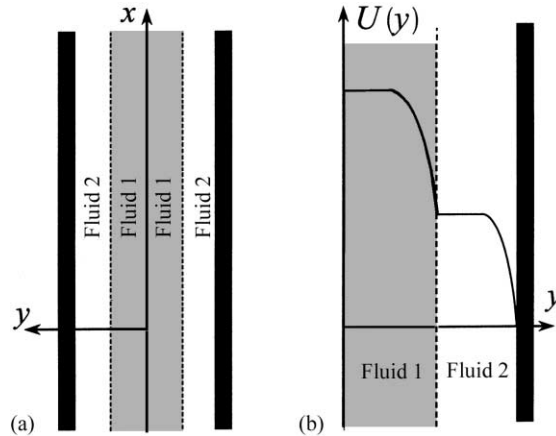


Fig. 1. Schematic view: (a) a symmetric two-layer multiple fluid flow; (b) a double Bingham–Poiseuille flow velocity profile in a half-slot.

static residual layer of displaced fluid to remain on the walls of the slot. The static residual layer is (near) parallel and falls into the class of flows which we consider.

The approach taken throughout the paper is mathematical rather than physical. To ease the reader's task, we summarise here the main threads of our analysis, in physical terms.

- We assume throughout the paper that the yield stresses of the two fluids satisfy $\hat{\tau}_{\text{yield}}^{[2]} > \hat{\tau}_{\text{yield}}^{[1]} \geq 0$. This constraint allows multi-layer flows to exist with velocity profiles such as that shown schematically in Fig. 1b. It is this type of profile that is responsible for the enhanced stability.
- With the velocity profile as indicated, the flows in each layer effectively uncouple, at least as far as the linear stability problem is concerned. Uncoupling occurs partly because the shear stress at the interface does not exceed the yield stress of fluid 2 (see Fig. 1), and therefore the interface is not deformed.
- On its own, the above is not sufficient to decouple the flows. However, by using analytical continuation of the sheared velocity field and continuity of the stress fields where indeterminate, it is possible to derive integral conditions describing the motion of the unyielded plug regions. For periodic linear perturbations, as found in a normal mode expansion, these integral terms vanish, leaving the unyielded regions unperturbed by the perturbation. This feature and the fact that the interface is not deformed, allows the two sheared flow regions to be completely uncoupled.
- Having uncoupled the two sheared flow regions, we are able to show that the stability problem in each fluid layer is in fact equivalent to that of a single Bingham fluid flow, as addressed in [15]. This equivalence is demonstrated via a simple but elegant transformation, which has the effect of reducing the Reynolds number and increasing the Bingham number. It is these two effects that result in increased stability of the multi-layer flow.

Although the two-layer Bingham–Poiseuille problem does not appear to have been studied before, Comparini and Mannucci [16] have recently considered the *reverse* of our lubrication flow configuration, whereby a Newtonian fluid lubricates a Bingham fluid. In [16] the focus is on the one-dimensional non-linear perturbation of the base flow. A number of results are proven related to the existence, uniqueness and stability of solutions to this one-dimensional transient problem. Since in this paper the lubricating

fluid must have a yield stress, whereas the lubricated fluid need not, the results in [16] are not directly applicable. It is thought that the configuration studied in [16], which results in an interface between the yielded Bingham fluid and the Newtonian fluid, would suffer from the classical interfacial instabilities described above.

However, the methods developed in [16] could be generalised to the study of one-dimensional non-linear perturbations of the two-layer flows considered here.

An outline of the paper is as follows. In the following section, we present the two-dimensional model for the flow and consider the basic flows. Section 3 considers linear periodic perturbations of the basic flow. In Section 4, the Orr–Sommerfeld eigenvalue problems for both fluid layers are derived. Section 4.3 shows how each problem can be transformed into an equivalent eigenvalue problem for a single Bingham fluid. Section 5.2 examines how to stabilise the flow of a Newtonian fluid by careful choice of the rheology of a Bingham fluid, to be used as a lubricant. The paper concludes in Section 6 with a discussion of the principal results and certain limitations to the analysis.

2. Multi-layer Bingham–Poiseuille flows

Consider a two-dimensional geometry between two infinitely long parallel plates, i.e. a slot. The slot is filled with two Bingham fluids: fluid 1 occupying the centre of the slot and fluid 2 adjacent to the walls. These fluids are characterised rheologically by their yield stresses, $\hat{\tau}_{\text{yield}}^{[k]}$, $k = 1, 2$, and plastic viscosities, $\hat{\mu}^{[k]}$, $k = 1, 2$. The two fluids have the same density $\hat{\rho}$. The fluids are assumed miscible, but we shall consider that the flow takes place on a timescale which does not allow significant molecular diffusion. Equivalently, we can assume that the fluids are immiscible and that surface tension effects at the interface are negligible. Cartesian co-ordinates (x, y) are as shown in Fig. 1a. For simplicity, only layered flows that are symmetric about the x -axis are considered. Both fluids move in the positive x -direction under the action of a constant pressure gradient. The areal flow rate, obtained by integrating the x -component of velocity across the slot, is denoted by $2\hat{D}\hat{U}_0$, where $2\hat{D}$ is the width of the slot, i.e. \hat{U}_0 is the mean speed in the slot. We assume throughout the paper that $\hat{\tau}_{\text{yield}}^{[2]} > \hat{\tau}_{\text{yield}}^{[1]} \geq 0$. Depending on the exact rheological parameters and the interface position, a velocity profile such as that in Fig. 1b can exist, which we refer to as a *double Bingham–Poiseuille* profile. In this paper, we consider the stability of basic velocity profiles: $\mathbf{u} = (u, v) = (U(y), 0)$, with $U(y)$ as illustrated in Fig. 1b.

Dimensionless equations of motion for the fully two-dimensional flow are

$$\frac{\partial u}{\partial t} + u \frac{\partial u}{\partial x} + v \frac{\partial u}{\partial y} = -\frac{\partial p^{[k]}}{\partial x} + \frac{\partial}{\partial x} \tau_{xx}^{[k]} + \frac{\partial}{\partial y} \tau_{xy}^{[k]}, \quad (1)$$

$$\frac{\partial v}{\partial t} + u \frac{\partial v}{\partial x} + v \frac{\partial v}{\partial y} = -\frac{\partial p^{[k]}}{\partial y} + \frac{\partial}{\partial x} \tau_{yx}^{[k]} + \frac{\partial}{\partial y} \tau_{yy}^{[k]}, \quad (2)$$

$$\frac{\partial u}{\partial x} + \frac{\partial v}{\partial y} = 0. \quad (3)$$

The modified pressure and deviatoric stresses tensors are denoted $p^{[k]}$ and $\tau_{ij}^{[k]}$, respectively, and the index superscript k is used where necessary, to distinguish the variables relating to the different fluids. Velocities have been scaled with \hat{U}_0 and lengths scaled with \hat{D} . The stress scale is $\hat{\rho}\hat{U}_0^2$. The interface position is

denoted $y = y_i(x, t)$ and is governed by the following kinematic equation:

$$\frac{\partial y_i}{\partial t} + \mathbf{u} \frac{\partial y_i}{\partial x} = v. \quad (4)$$

Across the interface both the velocity and traction vectors are continuous. The fluids are modelled by the following scaled constitutive laws:

$$\dot{\gamma}(\mathbf{u}) = 0 \Leftrightarrow \tau^{[k]}(\mathbf{u}) \leq \tau_{\text{yield}}^{[k]}, \quad (5)$$

$$\tau_{ij}^{[k]}(\mathbf{u}) = \left[\mu^{[k]} + \frac{\tau_{\text{yield}}^{[k]}}{\dot{\gamma}(\mathbf{u})} \right] \dot{\gamma}_{ij}(\mathbf{u}) \Leftrightarrow \tau^{[k]}(\mathbf{u}) > \tau_{\text{yield}}^{[k]}. \quad (6)$$

The dimensionless yield stresses $\tau_{\text{yield}}^{[k]}$ and plastic viscosities $\mu^{[k]}$ are defined by

$$\tau_{\text{yield}}^{[k]} \equiv \frac{\hat{\tau}_{\text{yield}}^{[k]}}{\hat{\rho} \hat{U}_0^2}, \quad \mu^{[k]} \equiv \frac{\hat{\mu}^{[k]}}{\hat{\rho} \hat{U}_0 \hat{D}}. \quad (7)$$

Rate of strain and deviatoric stress second invariants, $\dot{\gamma}(\mathbf{u})$ and $\tau^{[k]}(\mathbf{u})$, respectively, are defined by

$$\dot{\gamma}(\mathbf{u}) = \left[\frac{1}{2} \sum_{i,j=1}^2 [\dot{\gamma}_{ij}(\mathbf{u})]^2 \right]^{1/2}, \quad \tau^{[k]}(\mathbf{u}) = \left[\frac{1}{2} \sum_{i,j=1}^2 [\tau_{ij}^{[k]}(\mathbf{u})]^2 \right]^{1/2}, \quad (8)$$

where $x \equiv x_1$, $y \equiv x_2$, $u \equiv u_1$, $v \equiv u_2$ and

$$\dot{\gamma}_{ij}(\mathbf{u}) = \frac{\partial u_i}{\partial x_j} + \frac{\partial u_j}{\partial x_i}, \quad i, j = 1, 2. \quad (9)$$

2.1. Basic flows

We will consider the stability of an entire family of basic parallel shear flows, that are parameterised by $Y_i \in [0, 1]$, and which include the following double Bingham–Poiseuille profile:

$$U(y) = \begin{cases} U_p^{[2]} + U_p^{[1]}, & y \in [0, Y_{\text{yield}}^{[1]}], \\ U_p^{[2]} + U_p^{[1]} \left[1 - \frac{(y - Y_{\text{yield}}^{[1]})^2}{(Y_i - Y_{\text{yield}}^{[1]})^2} \right], & y \in (Y_{\text{yield}}^{[1]}, Y_i], \\ U_p^{[2]}, & y \in [Y_i, Y_{\text{yield}}^{[2]}], \\ U_p^{[2]} \left[1 - \frac{(y - Y_{\text{yield}}^{[2]})^2}{(1 - Y_{\text{yield}}^{[2]})^2} \right], & y \in (Y_{\text{yield}}^{[2]}, 1]. \end{cases} \quad (10)$$

With reference to (10) and the profile shown schematically in Fig. 1, $Y_{\text{yield}}^{[1]}$ and $Y_{\text{yield}}^{[2]}$ are the positions yield surfaces in each fluid layer. The velocities of the unyielded *plug* regions are denoted $U_p^{[1]}$ and $(U_p^{[2]} + U_p^{[1]})$, in fluids 1 and 2, respectively. The interface position is given by $y = Y_i$.

The basic flow $(U(y), 0)$, is a one-dimensional multi-layer shear flows. The axial pressure gradient is constant and strictly negative, with absolute value denoted by f . The solution (10) is computed from

$$\frac{d}{dy} \tau_{xy}^{[1]} = -f, \quad y \in [0, Y_i), \quad (11)$$

$$\frac{d}{dy} \tau_{xy}^{[2]} = -f, \quad y \in (Y_i, 1], \quad (12)$$

with the simplified constitutive relations

$$|U_y| = 0 \Leftrightarrow |\tau_{xy}^{[k]}| \leq \tau_{\text{yield}}^{[k]}, \quad k = 1, 2, \quad (13)$$

$$\tau_{xy}^{[k]} = \left[\mu^{[k]} + \frac{\tau_{\text{yield}}^{[k]}}{|U_y|} \right] U_y \Leftrightarrow |\tau_{xy}^{[k]}| > \tau_{\text{yield}}^{[k]}, \quad k = 1, 2, \quad (14)$$

The following boundary and interface conditions are satisfied:

$$\tau_{xy}^{[1]}(0) = 0, \quad U(1) = 0, \quad (15)$$

$$U(Y_i^-) = U(Y_i^+), \quad \tau_{xy}^{[1]}(Y_i^-) = \tau_{xy}^{[2]}(Y_i^+). \quad (16)$$

Finally, because the velocity scaling has been chosen as the mean velocity, the following condition must also be satisfied:

$$\int_0^1 U(y) dy = 1. \quad (17)$$

Constraint (17) is used to define f and the solution to (11)–(17) is consequently the pair (U, f) . It is known that there exists a unique solution (U, f) to this system for each value of $Y_i \in [0, 1]$, see e.g. [17]. For fixed parameters $(\tau_{\text{yield}}^{[1]}, \tau_{\text{yield}}^{[2]}, \mu^{[1]}, \mu^{[2]})$, the solution (U, f) will vary as Y_i varies in $[0, 1]$, giving a family of velocity profiles and values of $f = f(Y_i)$.

We denote by f_0 and f_1 the values of $f = f(Y_i)$, for $Y_i = 0$ and $Y_i = 1$, respectively. After some analysis we are able to distinguish three distinct qualitatively different families of velocity profile solutions. These three families are distinguished by the values of f_1 , by the fluid 1 Bingham number, B_1 , by the yield stress ratio, φ_Y , and by the condition (18) below.

$$\frac{\mu^{[1]}}{\mu^{[2]}} > \frac{f_1 - \tau_{\text{yield}}^{[1]}}{f_1 - \tau_{\text{yield}}^{[2]}}. \quad (18)$$

The fluid 1 Bingham number and yield stress ratio are defined by

$$B_1 = \frac{\tau_{\text{yield}}^{[1]}}{\mu^{[1]}}, \quad \varphi_Y = \frac{\tau_{\text{yield}}^{[1]}}{\tau_{\text{yield}}^{[2]}}. \quad (19)$$

Omitting the lengthy analysis, the three families are

1. $f_1 < \tau_{\text{yield}}^{[2]}$. In this case, the family of solutions consists of unyielded fluid 1 layers for interfaces Y_i close to $Y_i = 0$, followed by an interval of double Bingham–Poiseuille velocity profiles, followed by an interval of static wall layer velocity profiles, i.e. the fluid 2 layer is static. The static wall layers are found for $Y_i \in [Y_{i,\min}, 1]$, where $Y_{i,\min} = Y_{i,\min}(B_1, \varphi_Y)$ is easily computed. The function $f(Y_i)$ decreases from f_0 to f_1 .
2. $f_1 > \tau_{\text{yield}}^{[2]}$ and (18) is not satisfied. In this case, the family of solutions consists of unyielded fluid 1 layers for interfaces Y_i close to $Y_i = 0$, followed by an interval of double Bingham–Poiseuille velocity profiles, followed by an interval of velocity profiles for which the fluid 2 layer is completely sheared. The function $f(Y_i)$ decreases from f_0 to f_1 .
3. $f_1 > \tau_{\text{yield}}^{[2]}$ and (18) is satisfied. In this case, the family of solutions consists of unyielded fluid 1 layers for interfaces Y_i close to $Y_i = 0$, followed by an interval of double Bingham–Poiseuille velocity profiles, followed by an interval of velocity profiles for which the fluid 2 layer is completely sheared. The function $f(Y_i)$ decreases throughout the first two intervals, but increases in a small interval close to $Y_i = 1$ where the fluid 2 layer is fully sheared. This small interval is where classical fluid lubrication occurs.

The remainder of this paper will concern only the first of these families. Parametrically, this family of solutions occupies a well-defined region in the (B_1, φ_Y) -plane, in which $Y_{i,\min} < 1$. This region is the contoured region illustrated in Fig. 2. The other two families of solutions occupy the shaded region in Fig. 2, delineated via the ratio of plastic viscosities and condition (18).

As an example of the type of family we will consider, Fig. 3 shows computed variations in f_i in the interfacial shear stress, $\tau_i \equiv \tau_{xy}^{[1]}(Y_i) = \tau_{xy}^{[2]}(Y_i)$, and in the two plug velocities $U_p^{[1]}$ and $U_p^{[2]}$, each for $Y_i \in [0, 1]$. Note that for the initial interval of unyielded fluid 1, we define $U_p^{[1]} = 0$, and for the static wall-layer

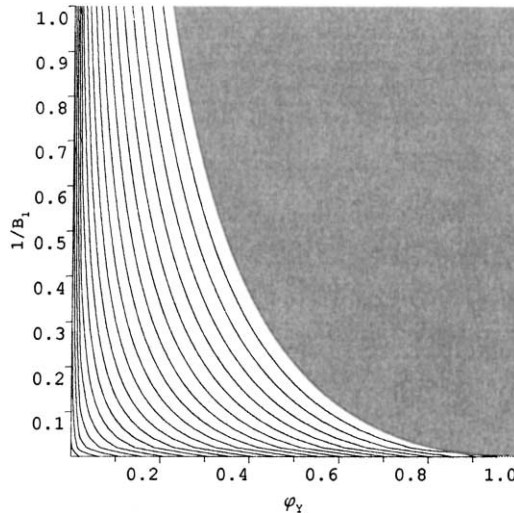


Fig. 2. Contour plot of the function $1 - Y_{i,\min}(B_1, \varphi_Y)$: contour spacing at intervals $\Delta = 0.05$, the shaded area illustrates the region where $Y_{i,\min}(B_1, \varphi_Y) = 1$.

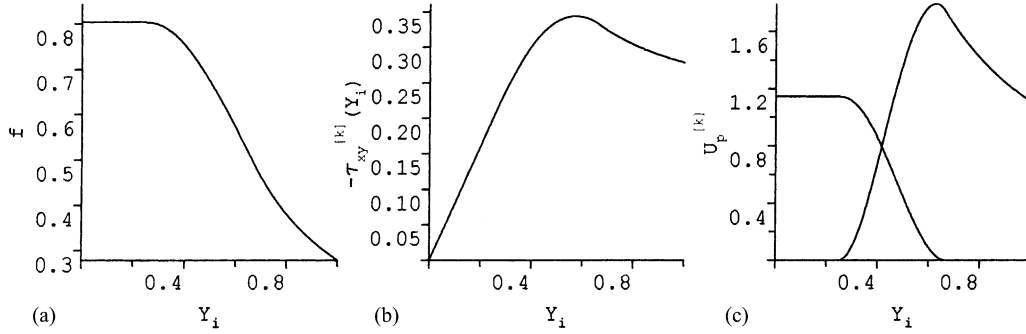


Fig. 3. Example of computed variations with Y_i : (a) $f(Y_i)$; (b) $\tau_{xy}^{[k]}(Y_i)$; (c) $U_p^{[1]}(Y_i)$ and $U_p^{[2]}(Y_i)$ ($U_p^{[1]}$ is decreasing). Rheological parameters are $(\tau_{yield}^{[1]}, \tau_{yield}^{[2]}, \mu^{[1]}, \mu^{[2]}) = (0.2, 0.5, 0.01, 0.05)$.

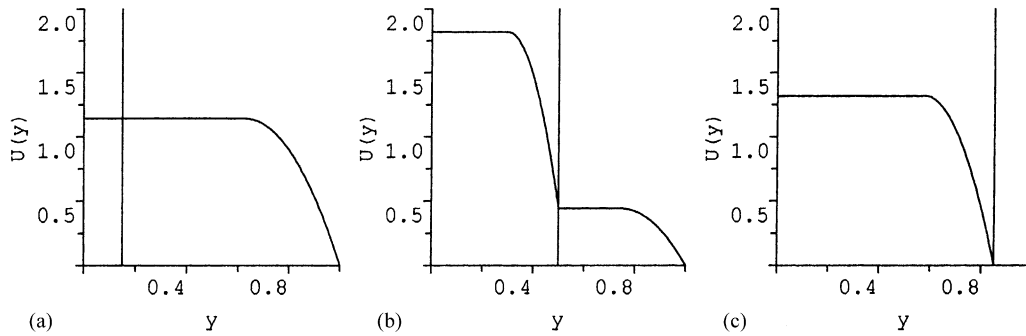


Fig. 4. Example velocity profiles at different Y_i for fixed rheological parameters $(\tau_{yield}^{[1]}, \tau_{yield}^{[2]}, \mu^{[1]}, \mu^{[2]}) = (0.2, 0.5, 0.01, 0.05)$: (a) $Y_i = 0.15$, fluid 1 is unyielded; (b) $Y_i = 0.5$, the double Bingham–Poiseuille profile; (c) $Y_i = 0.85$, fluid 2 is unyielded. Interface position is marked with the vertical line.

velocity profiles, we define $U_p^{[2]} = 0$. With this interpretation, (10) defines the velocity profile for all $Y_i \in [0, 1]$. The parameters for this example are fixed at $(\tau_{yield}^{[1]}, \tau_{yield}^{[2]}, \mu^{[1]}, \mu^{[2]}) = (0.2, 0.5, 0.01, 0.05)$. The three distinct sub-intervals of $Y_i \in [0, 1]$ can easily be identified. The intermediate sub-interval with velocity profiles exactly as in (10) is identified by positive values of both $U_p^{[1]}$ and $U_p^{[2]}$. In Fig. 4, we show an example of a velocity profile computed in each of these sub-intervals.

3. Linear x-periodic perturbations of the basic flow

We turn now to the stability of (10) to one- and two-dimensional linear disturbances. Our analysis is only fully applicable to families of basic flows with rheological parameters which lie in the contoured area of Fig. 2, i.e. families of velocity solutions as illustrated qualitatively in Figs. 3 and 4. For other families of solutions, our analysis is not valid for interfaces close to the wall, but will be valid for the double-Bingham Poiseuille flows.

In this section, we present the linear perturbation equations for the two-fluid flow. A key question concerns the effect of a perturbation on the unyielded plug regions. Two-dimensional linear instabilities of axial shear flows are governed by the Orr–Sommerfeld equation, which defines a fourth-order complex eigenvalue problem. The exact form of the Orr–Sommerfeld equation depends upon the fluid rheology and underlying flow. To derive this equation, we assume a completely symmetric basic flow and consider only $y \in [0, 1]$. The solution to the two-dimensional equations is the vector (u, v, p, y_i) , which is assumed to have the form

$$(u, v, p, y_i) = (U + \epsilon \tilde{u}, V + \epsilon \tilde{v}, P + \epsilon \tilde{p}, Y_i + \epsilon \tilde{y}_i) \quad (20)$$

where $\epsilon \ll 1$ and the basic flow is

$$U = U(y),$$

$$V = 0,$$

$$P = -fx + \text{constant},$$

$$Y_i = \text{constant}.$$

To derive linear perturbation equations, note first that the basic solution is a solution to the complete set of Eqs. (1)–(6), with the boundary conditions discussed. Strictly speaking, the linearised equations are derived only for yielded regions of both perturbed and unperturbed flows, since elsewhere the stress field is indeterminate. The yielded region of the perturbed flow is however linearised onto the yielded region of the unperturbed flow. In yielded parts of the flow, the deviatoric stress tensor may be written as

$$\tau_{ij}^{[k]} = \tau_{ij}^{[k]}(\mathbf{u}) = \eta^{[k]}(\mathbf{u}) \dot{\gamma}_{ij}(\mathbf{u}), \quad (21)$$

where

$$\eta^{[k]}(\mathbf{u}) = \mu^{[k]} + \frac{\tau_{\text{yield}}^{[k]}}{\dot{\gamma}(\mathbf{u})} \quad (22)$$

and \mathbf{u} is a velocity vector, with associated rate of strain tensor $\dot{\gamma}_{ij}(\mathbf{u})$. With a little work, the linear perturbation of the shear stress tensor can be expanded about the basic flow:

$$\tau_{ij}^{[k]}(\mathbf{U} + \epsilon \tilde{\mathbf{u}}) - \tau_{ij}^{[k]}(\mathbf{U}) = \epsilon \eta^{[k]}(\mathbf{U}) \dot{\gamma}_{ij}(\tilde{\mathbf{u}}), \quad ij = xx, yy, \quad (23)$$

$$\tau_{ij}^{[k]}(\mathbf{U} + \epsilon \tilde{\mathbf{u}}) - \tau_{ij}^{[k]}(\mathbf{U}) = \epsilon \mu^{[k]} \dot{\gamma}_{ij}(\tilde{\mathbf{u}}), \quad ij = yx, xy. \quad (24)$$

(see e.g. [15]). The additional assumption is now made that

$$|\tau_{ij}^{[k]}(\mathbf{U} + \epsilon \tilde{\mathbf{u}}) - \tau_{ij}^{[k]}(\mathbf{U})| = O(\epsilon). \quad (25)$$

The physical relevance of (25) is that the perturbed flow can only *linearly* perturb the yield surfaces from their initial positions. Therefore, this will leave an unyielded plug region in the interior of the perturbed flow. Mathematically, (25) can be viewed as specifying a more restrictive norm for the perturbation. Note that

$$|\tau^{[k]}(\mathbf{U} + \epsilon \tilde{\mathbf{u}}) - \tau^{[k]}(\mathbf{U})| = O(\epsilon) \Rightarrow \dot{\gamma}(\tilde{\mathbf{u}}) = O(1), \quad (26)$$

from which it is clear that the perturbation is assumed to be $O(\epsilon)$ in the H^1 norm, instead of the usual L^2 norm. In place of (25), it could have been assumed that the perturbation is $O(\epsilon)$ in the H^1 norm, but this would not imply (25) for a Bingham fluid since the stress is indeterminate below the yield stress. For a Newtonian fluid these norms are equivalent and perhaps the best way of viewing (25) is as a more *natural* norm to use for a perturbation of a Bingham fluid flow. These points may seem insignificant, but note that if we are unable to linearise the yielded region of the perturbed flow onto that of the basic flow it is doubtful that a linear stability analysis can be carried out for a true Bingham fluid.

Assuming (25), the leading order perturbed flow regions are simply the yielded regions of the basic flow: $y \in (Y_{\text{yield}}^{[1]}, Y_i)$ for fluid 1 and $y \in (Y_{\text{yield}}^{[2]}, 1)$ for fluid 2. In each region the following linear equations result:

$$\tilde{u}_t + U\tilde{u}_x + \tilde{v}U_y = -\tilde{p}_x + \mu^{[k]}[\tilde{u}_{xx} + \tilde{u}_{yy}] + 2\tau_{\text{yield}}^{[k]} \frac{\tilde{u}_{xx}}{|U_y|}, \quad (27)$$

$$\tilde{v}_t + U\tilde{v}_x = -\tilde{p}_y + \mu^{[k]}[\tilde{v}_{xx} + \tilde{v}_{yy}] + 2\tau_{\text{yield}}^{[k]} \frac{\partial}{\partial y} \left[\frac{\tilde{v}_y}{|U_y|} \right], \quad (28)$$

$$\tilde{u}_x + \tilde{v}_y = 0. \quad (29)$$

3.1. Boundary, interface and yield surface conditions

Conditions at $y = 1$ come directly from the no slip conditions at the wall

$$\tilde{u}(x, 1, t) = 0, \quad (30)$$

$$\tilde{v}(x, 1, t) = 0. \quad (31)$$

The yield surface for the perturbed flow in fluid 2 is denoted $y = Y_{\text{yield}}^{[2]} + \epsilon\tilde{y}^{[2]}$. Therefore, at $y = Y_{\text{yield}}^{[2]} + \epsilon\tilde{y}^{[2]}$ we have

$$\dot{\gamma}(\mathbf{U} + \epsilon\tilde{\mathbf{u}}) = 0 \Rightarrow \dot{\gamma}_{ij}(\mathbf{U} + \epsilon\tilde{\mathbf{u}}) = 0, \quad \forall i, j. \quad (32)$$

Expanding and linearising onto $y = Y_{\text{yield}}^{[2]}$:

$$\tilde{u}_x(x, Y_{\text{yield}}^{[2]}, t) = 0, \quad (33)$$

$$\tilde{v}_y(x, Y_{\text{yield}}^{[2]}, t) = 0, \quad (34)$$

$$\tilde{u}_y(x, Y_{\text{yield}}^{[2]}, t) + \tilde{v}_x(x, Y_{\text{yield}}^{[2]}, t) = -\tilde{y}^{[2]}U''(Y_{\text{yield}}^{[2]}) = \frac{2\tilde{y}^{[2]}U_p^{[2]}}{(1 - Y_{\text{yield}}^{[2]})^2} = \frac{f\tilde{y}^{[2]}}{\mu^{[2]}}. \quad (35)$$

Also, at the yield surface the velocity vector is continuous. The perturbed velocity of the unyielded plug region is given by the vector

$$\mathbf{u} = (U_p^{[2]} + \epsilon u_p^{[2]}, \epsilon v_p^{[2]}), \quad (36)$$

where (note that there can be no spatial variation):

$$u_p^{[2]}(x, y, t) = u_p^{[2]}(t), \quad v_p^{[2]}(x, y, t) = v_p^{[2]}(t).$$

We linearise the velocity continuity condition about the basic solution and onto the yield surface at $y = Y_{\text{yield}}^{[2]}$:

$$\begin{aligned} U_p^{[2]} + \epsilon u_p^{[2]} &= U(Y_{\text{yield}}^{[2]} + \epsilon \tilde{y}^{[2]}) + \epsilon \tilde{u}(x, Y_{\text{yield}}^{[2]} + \epsilon \tilde{y}^{[2]}, t) \\ &= U(Y_{\text{yield}}^{[2]}) + \epsilon [\tilde{y}^{[2]} U'(Y_{\text{yield}}^{[2]}) + \tilde{u}(x, Y_{\text{yield}}^{[2]}, t)] + \mathcal{O}(\epsilon^2) \\ &= U_p^{[2]} + \epsilon \tilde{u}(x, Y_{\text{yield}}^{[2]}, t) + \mathcal{O}(\epsilon^2), \end{aligned}$$

arriving at

$$\tilde{u}(x, Y_{\text{yield}}^{[2]}, t) = u_p^{[2]}(t), \quad (37)$$

$$\tilde{v}(x, Y_{\text{yield}}^{[2]}, t) = v_p^{[2]}(t). \quad (38)$$

At the interface, both the traction and velocity vectors are continuous. However, fluid 2 is unyielded so that the stress is indeterminate within fluid 2. Thus, the stress continuity condition is not immediately useful. We linearise the velocity continuity conditions about the basic solution and onto the interface at $y = Y_i$:

$$\begin{aligned} U_p^{[2]} + \epsilon u_p^{[2]} &= U(Y_i + \epsilon \tilde{y}_i) + \epsilon \tilde{u}(x, Y_i + \epsilon \tilde{y}_i, t) = U(Y_i^-) + \epsilon [\tilde{y}_i U'(Y_i^-) + \tilde{u}(x, Y_i^-, t)] + \mathcal{O}(\epsilon^2) \\ &= U_p^{[2]} + \epsilon \left[-\frac{f \tilde{y}_i (Y_i - Y_{\text{yield}}^{[1]})}{\mu^{[1]}} + \tilde{u}(x, Y_i^-, t) \right] + \mathcal{O}(\epsilon^2), \end{aligned}$$

arriving at

$$\tilde{u}(x, Y_i^-, t) = u_p^{[2]}(t) + \frac{f \tilde{y}_i (Y_i - Y_{\text{yield}}^{[1]})}{\mu^{[1]}}, \quad (39)$$

$$\tilde{v}(x, Y_i^-, t) = v_p^{[2]}(t). \quad (40)$$

The linearised equation for the interface propagation comes directly from the kinematic condition at the interface:

$$\frac{\partial \tilde{y}_i}{\partial t} + U_p^{[2]} \frac{\partial \tilde{y}_i}{\partial x} = v_p^{[2]}. \quad (41)$$

The yield surface for the perturbed flow in fluid 1 perturbs to $y = Y_{\text{yield}}^{[1]} + \epsilon \tilde{y}^{[1]}$. Following the same steps as for fluid 2, we have

$$\tilde{u}_x(x, Y_{\text{yield}}^{[1]}, t) = 0, \quad (42)$$

$$\tilde{v}_y(x, Y_{\text{yield}}^{[1]}, t) = 0, \quad (43)$$

$$\tilde{u}_y(x, Y_{\text{yield}}^{[1]}, t) + \tilde{v}_x(x, Y_{\text{yield}}^{[1]}, t) = -\tilde{y}^{[1]} U''(Y_{\text{yield}}^{[1]}) = \frac{2\tilde{y}^{[1]} U_p^{[1]}}{(1 - Y_{\text{yield}}^{[1]})^2} = \frac{f \tilde{y}^{[1]}}{\mu^{[1]}}. \quad (44)$$

Finally, continuity conditions at the fluid 1 plug region give

$$\tilde{u}(x, Y_{\text{yield}}^{[1]}, t) = u_p^{[1]}(t), \quad (45)$$

$$\tilde{v}(x, Y_{\text{yield}}^{[1]}, t) = v_p^{[1]}(t), \quad (46)$$

where the plug velocity is now $\mathbf{u} = (U_p^{[1]} + U_p^{[2]} + \epsilon u_p^{[1]}, \epsilon v_p^{[1]})$.

3.2. Plug motion in two-dimensional x -periodic perturbations

To close the system we need to consider the motion of the plug regions. This is of critical importance in considering this type of stability problem for two reasons. First, the acceleration and motion of the perturbed plug region gives the boundary conditions for the perturbed velocity in fluid 1, see (37), (38), (45) and (46). Second, the plug motion determines whether or not the stability problems in the two-fluid layers are actually coupled. The conditions for the plug velocities in an arbitrary periodically and linearly perturbed flow are

$$\frac{d}{dt} u_p^{[1]} = \frac{\mu^{[1]}}{2XY_{\text{yield}}^{[1]}} \int_{-X}^X \tilde{u}_y(x, Y_{\text{yield}}^{[1]}, t) dx, \quad (47)$$

$$\frac{d}{dt} v_p^{[1]} = -\frac{1}{2XY_{\text{yield}}^{[1]}} \int_{-X}^X \tilde{p}_1(x, Y_{\text{yield}}^{[1]}, t) dx, \quad (48)$$

$$\frac{d}{dt} u_p^{[2]} = \frac{1}{2X(Y_{\text{yield}}^{[2]} - Y_i)} \int_{-X}^X [\mu^{[2]} \tilde{u}_y(x, Y_{\text{yield}}^{[2]}, t) - \mu^{[1]} \tilde{u}_y(x, Y_i, t)] dx, \quad (49)$$

$$\frac{d}{dt} v_p^{[2]} = \frac{1}{2X(Y_{\text{yield}}^{[2]} - Y_i)} \int_{-X}^X [\tilde{p}_1(x, Y_i, t) - \tilde{p}_2(x, Y_{\text{yield}}^{[2]}, t)] dx, \quad (50)$$

where the perturbation is assumed periodic over the arbitrary length $2X$ in the x -direction. Derivation of these conditions proceeds along the same lines as in [15].

Later, we will use a normal mode analysis. This type of analysis makes the distinction between perturbations that have zero-mean (i.e. non-zero wave-number) and those with a non-zero mean, which are effectively one-dimensional linear perturbations (see Section 3.3). For perturbations with zero mean, the integral terms in (47)–(50) vanish, leading to

$$\frac{d}{dt} u_p^{[k]} = \frac{d}{dt} v_p^{[k]} = 0, \quad k = 1, 2, \quad (51)$$

i.e. for non-zero wave-number the plug regions are not accelerated.

3.3. One-dimensional linear perturbations

Before proceeding in generality, we consider perturbations that are purely one-dimensional. A one-dimensional linear analysis assumes a perturbation of form

$$[\tilde{u}, \tilde{v}, \tilde{p}, \tilde{y}^{[1]}, \tilde{y}^{[2]}, \tilde{y}_i] = [u(y), v(y), p(y), \tilde{y}^{[1]}, \tilde{y}^{[2]}, \tilde{y}_i] e^{\lambda t},$$

with $\tilde{y}^{[1]}$, $\tilde{y}^{[2]}$ and \tilde{y}_i constants. The incompressibility equation and the boundary condition at the wall implies that $v(y) = 0$ in fluid 2. This gives that $v_p^{[2]} = 0$ and hence that $v(y) = 0$ in fluid 1. The momentum

equation then leads to $p(y) = \text{constant}$ and the kinematic condition gives that $\tilde{y}_i = 0$. This leaves only the x -momentum equation and the x -motion of the plug regions. The following system results:

$$\lambda u_p^{[1]} = \frac{\mu^{[1]} u_y(Y_{\text{yield}}^{[1]})}{Y_{\text{yield}}^{[1]}}, \quad (52)$$

$$\lambda u = \mu^{[1]} u_{yy}, \quad y \in (Y_{\text{yield}}^{[1]}, Y_i) : u(Y_{\text{yield}}^{[1]}) = u_p^{[1]}, \quad u(Y_i) = u_p^{[2]}, \quad (53)$$

$$\lambda u_p^{[2]} = \frac{\mu^{[2]} u_y(Y_{\text{yield}}^{[2]}) - \mu^{[1]} u_y(Y_i)}{Y_{\text{yield}}^{[2]} - Y_i}, \quad (54)$$

$$\lambda u = \mu^{[2]} u_{yy}, \quad y \in (Y_{\text{yield}}^{[2]}, 1) : u(Y_{\text{yield}}^{[2]}) = u_p^{[2]}, \quad u(1) = 0, \quad (55)$$

together with

$$\lambda u_p^{[1]} = \frac{\mu^{[1]} \tilde{u}_y(Y_{\text{yield}}^{[1]})}{Y_{\text{yield}}^{[1]}}, \quad (56)$$

$$\lambda u_p^{[2]} = \frac{\mu^{[2]} (Y_{\text{yield}}^{[2]}) - \mu^{[1]} \tilde{u}_y(Y_i)}{Y_{\text{yield}}^{[2]} - Y_i}, \quad (57)$$

Multiplying through by $u(y)$, integrating across each sheared fluid region integration, by parts, and finally using the above conditions on the plug motion, produces, straightforwardly

$$\lambda = - \frac{\mu^{[1]} \int_{Y_{\text{yield}}^{[1]}}^{Y_i} u_y^2(y) dy + \mu^{[2]} \int_{Y_{\text{yield}}^{[2]}}^1 u_y^2(y) dy}{\int_0^1 u^2(y) dy} \leq 0. \quad (58)$$

Therefore, we conclude that the one-dimensional perturbation is always linearly stable.

4. The Orr–Sommerfeld eigenvalue problem

We are now in a position to consider the two-dimensional eigenvalue problem. The incompressibility condition is satisfied by defining a stream function Ψ :

$$\tilde{u} = \Psi_y, \quad \tilde{v} = -\Psi_x, \quad (59)$$

and the pressure is then eliminated from the equations of momentum by cross-differentiation. This leaves a fourth-order equation for the stream function. We rewrite the stream function in normal mode form:

$$\Psi(x, y, t) = \phi_1(y) e^{i\alpha_1(x-c_1)t}, \quad y \in [Y_{\text{yield}}^{[1]}, Y_i], \quad (60)$$

$$\Psi(x, y, t) = \phi_2(y) e^{i\alpha_2(x-c_2)t}, \quad y \in [Y_{\text{yield}}^{[2]}, 1], \quad (61)$$

with $\alpha_k \neq 0$, and note that the assumption that the wave-numbers are identical is not necessarily made.

The plug velocities have no (x, y) -variation and therefore, we write

$$u_p^{[k]}(t) = \tilde{u}_p^{[k]} e^{-i\alpha_k c_k t}, \quad k = 1, 2, \quad (62)$$

$$v_p^{[k]}(t) = \tilde{v}_p^{[k]} e^{-i\alpha_k c_k t}, \quad k = 1, 2, \quad (63)$$

for constants $\tilde{u}_p^{[k]}$ and $\tilde{v}_p^{[k]}$. The yield surface perturbations are denoted

$$\tilde{y}^{[k]}(x, t) = \tilde{y}^{[k]} e^{i\alpha_k(x-c_k)t}, \quad k = 1, 2,$$

for constants $\tilde{y}^{[k]}$, $k = 1, 2$. Similarly, the interface perturbation we write as $\tilde{y}_i(x, t) = \tilde{y}_i e^{i\alpha_2(x-c_2)t}$, for a constant \tilde{y}_i .

Since the perturbations have zero mean, the plug motion equations imply

$$\tilde{u}_p^{[1]} = \tilde{v}_p^{[1]} = \tilde{u}_p^{[2]} = \tilde{v}_p^{[2]} = 0 \quad (64)$$

and we see from (41) that

$$[U_p^{[2]} - c_2]\tilde{y}_i = 0 \Rightarrow \tilde{y}_i = 0. \quad (65)$$

Thus, the interface position and the motion of the plug regions are not perturbed at leading order. These results appear to be physically sensible for an infinitesimal perturbation. Firstly, since the perturbations have zero mean and their effects are averaged along the length of the perturbed plug, it would be unlikely that the net effect of an infinitesimal perturbation can accelerate what is effectively an infinitely long piece of solid. Secondly, at the interface, fluid 2 is unyielded (by a finite amount). Consequently, an infinitesimal perturbation to fluid 1 which causes only an infinitesimal interfacial shear stress should not be able to disturb the basic state.

The consequence of these results is that the stability problems in the two fluid regions uncouple, in terms of their boundary conditions. The only form of coupling that remains in the stability problem is through the specification of the basic flow. This gives the different widths of the yielded flow regions and the velocity $U(y)$ in each yielded flow region. The Orr–Sommerfeld problems in the two fluid layers are as follows.

4.1. The Orr–Sommerfeld problem in fluid 1

The eigenvalue problem is

$$\begin{aligned} & \frac{i\alpha_1}{\mu^{[1]}} [(U - c_1)(\phi_{1,yy} - \alpha_1^2 \phi_1) - \phi_1 U_{yy}] \\ & = \left[\frac{d^2}{dy^2} - \alpha_1^2 \right]^2 \phi_1 - 4\alpha_1^2 \frac{\tau_{\text{yield}}^{[1]}}{\mu^{[1]}} \frac{d}{dy} \left[\frac{\phi_{1,y}}{|U_y|} \right], \quad \text{for } y \in (Y_{\text{yield}}^{[1]}, Y_i). \end{aligned} \quad (66)$$

Boundary conditions are

$$\phi_1(Y_{\text{yield}}^{[1]}) = \phi_{1,y}(Y_{\text{yield}}^{[1]}) = 0, \quad (67)$$

$$\phi_1(Y_i) = \phi_{1,y}(Y_i) = 0, \quad (68)$$

$$\phi_{1,yy}(Y_{\text{yield}}^{[1]}) - \alpha_1^2 \phi_1(Y_{\text{yield}}^{[1]}) = -\tilde{y}^{[1]} U_{yy}(Y_{\text{yield}}^{[1]}) = \frac{2\tilde{y}^{[1]} U_p^{[1]}}{(Y_i - Y_{\text{yield}}^{[1]})^2}. \quad (69)$$

These normal modes are unstable if $\text{Im}(c_1) > 0$. Note that although the interface and plug region are not perturbed, a linear perturbation of the yield surface is possible in (69).

4.2. The Orr–Sommerfeld problem in fluid 2

The eigenvalue problem is

$$\begin{aligned} & \frac{i\alpha_2}{\mu^{[2]}} [(U - c_2)(\phi_{2,yy} - \alpha_2^2 \phi_2) - \phi_2 U_{yy}] \\ & = \left[\frac{d^2}{dy^2} - \alpha_2^2 \right]^2 \phi_2 - 4\alpha_2^2 \frac{\tau_{\text{yield}}^{[2]}}{\mu^{[2]}} \frac{d}{dy} \left[\frac{\phi_{2,y}}{|U_y|} \right], \quad \text{for } y \in (Y_{\text{yield}}^{[2]}, 1). \end{aligned} \quad (70)$$

Boundary conditions are

$$\phi_1(Y_{\text{yield}}^{[2]}) = \phi_{1,y}(Y_{\text{yield}}^{[2]}) = 0, \quad (71)$$

$$\phi_1(1) = \phi_{1,y}(1) = 0, \quad (72)$$

$$\phi_{2,yy}(Y_{\text{yield}}^{[2]}) - \alpha_2^2 \phi_2(Y_{\text{yield}}^{[2]}) = -\tilde{y}^{[2]} U_{yy}(Y_{\text{yield}}^{[2]}) = \frac{2\tilde{y}^{[2]} U_p^{[2]}}{(1 - Y_{\text{yield}}^{[2]})^2}. \quad (73)$$

These normal modes are unstable if $\text{Im}(c_2) > 0$.

4.3. Transformed Orr–Sommerfeld problem

For the fluid 1 Orr–Sommerfeld problem we apply the following transformation:

$$\xi = \frac{y - Y_{\text{yield}}^{[1]}}{Y_i - Y_{\text{yield}}^{[1]}}, \quad (74)$$

$$\tilde{U}(\xi) = \frac{U(y(\xi)) - U_p^{[1]}}{U_p^{[1]}} = 1 - \xi^2, \quad (75)$$

$$\phi(\xi) = \phi_1(y(\xi)), \quad (76)$$

$$\alpha = (Y_i - Y_{\text{yield}}^{[1]})\alpha_1, \quad (77)$$

$$R = \frac{U_p^{[1]}(Y_i - Y_{\text{yield}}^{[1]})}{\mu^{[1]}}, \quad (78)$$

$$B = \frac{\tau_{\text{yield}}^{[1]}(Y_i - Y_{\text{yield}}^{[1]})}{\mu^{[1]}U_p^{[1]}}, \quad (79)$$

$$\text{Im}(c) = \frac{\text{Im}(c_1)}{U_p^{[1]}}, \quad (80)$$

$$\text{Re}(c) = \frac{\text{Re}(c_1) - U_p^{[2]}}{U_p^{[1]}}, \quad (81)$$

$$h = 2\tilde{y}^{[1]}U_p^{[1]}. \quad (82)$$

Similarly, for the fluid 2 Orr–Sommerfeld problem we apply the following transformation:

$$\xi = \frac{y - Y_{\text{yield}}^{[2]}}{1 - Y_{\text{yield}}^{[2]}}, \quad (83)$$

$$\tilde{U}(\xi) = \frac{U(y(\xi))}{U_p^{[2]}} = 1 - \xi^2, \quad (84)$$

$$\phi(\xi) = \phi_2(y(\xi)), \quad (85)$$

$$\alpha = (1 - Y_{\text{yield}}^{[2]})\alpha_2, \quad (86)$$

$$R = \frac{U_p^{[2]}(1 - Y_{\text{yield}}^{[2]})}{\mu^{[2]}}, \quad (87)$$

$$B = \frac{\tau_{\text{yield}}^{[2]}(1 - Y_{\text{yield}}^{[2]})}{\mu^{[2]}U_p^{[2]}}, \quad (88)$$

$$\text{Im}(c) = \frac{\text{Im}(c_2)}{U_p^{[2]}}, \quad (89)$$

$$\text{Re}(c) = \frac{\text{Re}(c_2)}{U_p^{[2]}}, \quad (90)$$

$$h = 2\tilde{y}^{[2]}U_p^{[2]}. \quad (91)$$

Both the Orr–Sommerfeld problems transform into

$$i\alpha R[(1 - \xi^2 - c)(\phi_{\xi\xi\xi} - \alpha^2\phi) + 2\phi] = \left[\frac{d^2}{d\xi^2} - \alpha^2 \right]^2 \phi - 2\alpha^2 B \frac{d}{d\xi} \left[\frac{\phi_\xi}{\xi} \right], \quad (92)$$

for $\xi \in (0, 1)$, with boundary conditions

$$\phi(0) = \phi_\xi(0) = 0, \quad (93)$$

$$\phi(1) = \phi_\xi(1) = 0, \quad (94)$$

$$\phi_{\xi\xi\xi}(0) - \alpha^2\phi(0) = 2h. \quad (95)$$

This problem is exactly the same eigenvalue problem as for the linear stability of Poiseuille flow of a single Bingham fluid, studied in [15]. Note that the normal modes of the above problem are unstable if

$\text{Im}(c) > 0$, in which case the normal modes of both the transformed problems will also be unstable, i.e. not only do the two problems transform into an identical eigenvalue problem, but the stability criterion is also preserved by the transformation.

4.4. Example results

The Orr–Sommerfeld problems (92)–(95) is solved using the methods in [15]. For each fixed B we can construct the marginal stability curve on which $\text{Im}(c) = 0$ (see Fig. 5a), and on each curve we are able to compute the minimum critical Reynolds number R_c ; here we have used a bisection method. We show the

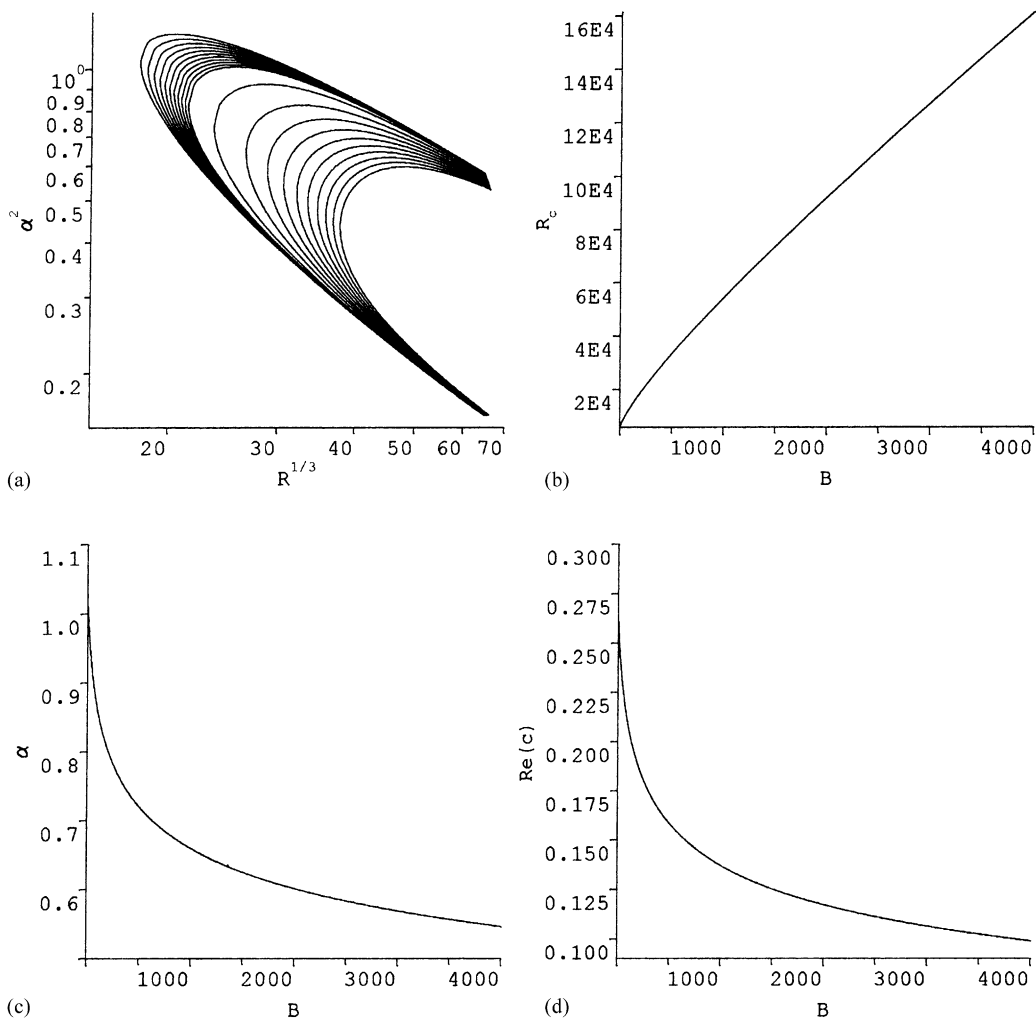


Fig. 5. Results from the Orr–Sommerfeld problems (92)–(95): (a) marginal stability curves for $B = 0, 5, 10, 15, 20, 25, 30, 35, 40, 45, 50, 100, 200, 300, 400, 500, 600, 700, 800, 900, 1000$; (b) critical Reynolds number $R_c(B)$, computed at $B = B_j \equiv 5 \times j : j = 0, \dots, 800$; (c) wave-number at critical Reynolds number; (d) $\text{Re}(c)$ at critical Reynolds number.

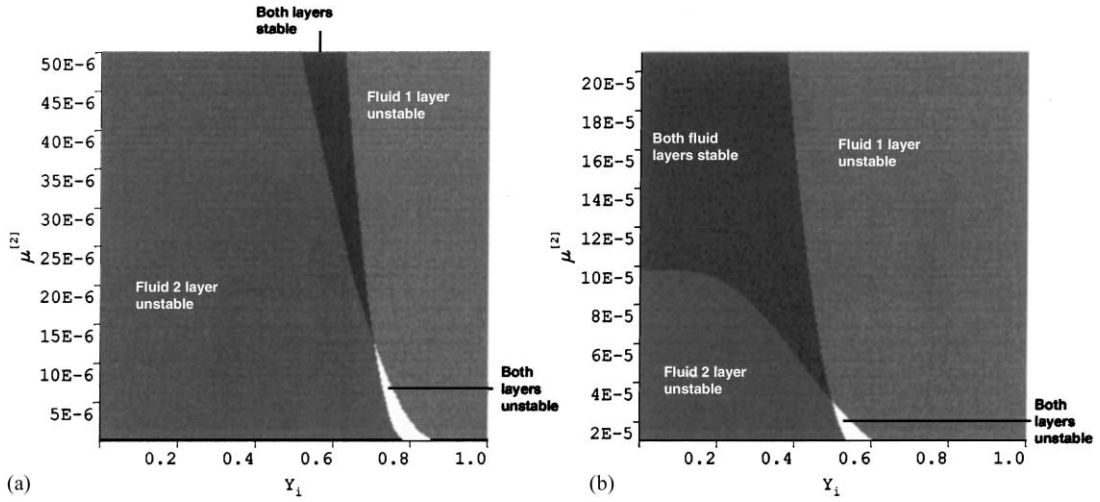


Fig. 6. Linearly stable and unstable regions for both fluid layers: (a) $\tau_{\text{yield}}^{[1]} = 0.0002$, $\tau_{\text{yield}}^{[2]} = 0.005$, $\mu^{[1]} = 0.0005$, $\mu^{[2]} \in [0.00000005, 0.0005]$; (b) $\tau_{\text{yield}}^{[1]} = 0.0001$, $\tau_{\text{yield}}^{[2]} = 0.005$, $\mu^{[1]} = 0.0005$, $\mu^{[2]} \in [0.00001, 0.00021]$.

results of these computations in Fig. 5b, where we have computed $R_c(B)$ for 800 equally spaced values of B in the range ¹ $B \in [0, 4000]$. Fig. 5c and d show the values of α and $Re(c)$, respectively, at the critical Reynolds number for these same values of B .

The transform of Section 4.3 directly defines the linear stability of the two-layer flow, in terms of the single fluid stability problems (92)–(95). Full exploration of the linearly stable and unstable regimes in the five-dimensional parameter space $(\tau_{\text{yield}}^{[1]}, \tau_{\text{yield}}^{[2]}, \mu^{[1]}, \mu^{[2]}, Y_i)$, is a significant task and of questionable practical value. However, it is clear that one or both fluid layers can be either stable or unstable, for different Y_i . We present two examples in Fig. 6 which illustrate this complexity. For fixed $(\tau_{\text{yield}}^{[1]}, \tau_{\text{yield}}^{[2]}, \mu^{[1]})$, Fig. 6 shows the variation of stable and unstable regimes in the $(Y_i, \mu^{[2]})$ -plane. For the parameter ranges chosen, we can find regions where either fluid layer can be unstable alone, separated by regions where either both fluids are stable or unstable. Note that for stability of the entire flow, we would require that both layers be stable.

5. Improved stability of the multi-layer flow

Individual results such as presented in Fig. 6 are of limited practical value, although of mathematical interest. From the practical perspective, we would like to know whether or not the multi-layer flows are more or less stable than single fluid flows of either fluid, since this opens up possibilities of lubricated

¹ As an aside, we note that the asymptotic behaviour of $R_c(B)$ as $B \rightarrow \infty$ is an interesting sub-problem that has not been studied. For a single fluid this problem represents the limit of an increasingly thin layer of yielded fluid at the walls. The computations that we have presented extend the range of the results in [15] considerably, but we still run into numerical problems at large B . An asymptotic analysis would be both interesting and complementary. On close examination the behaviour of $R_c(B)$ in Fig. 5b is not quite linear, as conjectured in [15], but perhaps $B \approx 4000$ is not *large enough* for $R_c(B)$ to have closely approached its asymptotic limit.

transport via a multi-layer flow. We note that the flows we consider are certainly more stable than would be analogous multi-layer flows with fluids for which fluid 2 does not have a yield stress, simply because we have eliminated the possibility of linear interfacial instabilities, e.g. Newtonian multi-layer flows. Thus, here we are considering whether, in addition to this already significant gain in stability, we can also improve the stability of the shear flows.

In Section 5.1, we examine the general effects of the transforms of Section 4.3 on multi-layer Bingham fluid flows. We then relax the constraint that fluid 1 have a yield stress and consider, in Section 5.2, the simplified problem of whether or not a Newtonian fluid can be lubricated stably by a Bingham fluid at the walls, i.e. can we transport a fixed flow rate of fluid 1 at a significantly reduced Reynolds number by introducing a thin layer of a suitably chosen fluid 2 at the walls?

5.1. General effects

By applying the transforms of Section 4.3, the linear stability of each fluid layer becomes equivalent to the linear stability of the single fluid Bingham–Poiseuille problems (92)–(95). Each individual fluid problem, (66)–(69) and (70)–(73), gives rise to different values of R and B , at each Y_i . If we apply the transforms of Section 4.3 at either $Y_i = 1$ or 0 , the Reynolds and Bingham numbers that we recover correspond to those for the single fluid flow, of either fluid 1 or 2, respectively. Our assertion is that it is always possible to achieve *improved stability* of the multi-layer flow, over an interval of intermediate values of Y_i . By improved stability is implied the following, for each Y_i in the interval.

- The effective Reynolds numbers R , for each individual fluid layer are smaller than the Reynolds numbers of each fluid were it to flow alone (i.e. taking $Y_i = 1$ or 0 , for fluid 1 or 2, respectively).
- The effective Bingham numbers B , for each individual fluid layer, are larger than the Bingham numbers of each fluid were it to flow alone (i.e. taking $Y_i = 1$ or 0 , for fluid 1 or 2, respectively).

Since the critical Reynolds number for linear instability increases with B , see Fig. 5b, both the above effects imply a move away from a linearly unstable flow. As an example of this reduction in R and increase in B , Fig. 7 plots the variation of R and B with Y_i (in each fluid), for rheological parameters $(\tau_{\text{yield}}^{[1]}, \tau_{\text{yield}}^{[2]}, \mu^{[1]}, \mu^{[2]}) = (0.1, 0.5, 0.01, 0.001)$. It can be seen in Fig. 7a that the fluid 1 Reynolds number is initially zero, then increases with Y_i throughout the double Bingham–Poiseuille profile regime, up to the limit $Y_{i,\text{min}}$. It then decreases throughout the static layer regime attaining its single fluid value

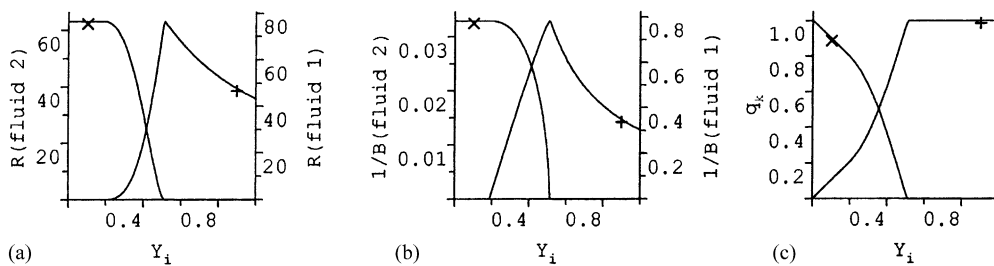


Fig. 7. Variations with Y_i : (a) R for each fluid, following the transformations of Section 4.3; (b) B for each fluid, following the transformations of Section 4.3; (c) q_1 and q_2 . Rheological parameters are $(\tau_{\text{yield}}^{[1]}, \tau_{\text{yield}}^{[2]}, \mu^{[1]}, \mu^{[2]}) = (0.1, 0.5, 0.01, 0.001)$. Fluid 1 marked with '+', fluid 2 marked with 'x'.

at the wall, $Y_i = 1$. The fluid 2 Reynolds number is constant for small Y_i and then decreases throughout the double Bingham–Poiseuille profile regime, to zero at the limit $Y_{i,\min}$. The same trend is followed by $1/B$ for both fluids, see Fig. 7b.

The interval of improved stability is found within the central double Bingham–Poiseuille regime, where the fluid 1 Reynolds number is below its value at the wall. The same qualitative behaviour as in Fig. 7 is found for all rheological parameters that admit families of velocity profile solutions of the type we have considered, i.e. defined by the contoured region in Fig. 2. To understand how improved stability arises from the transforms of Section 4.3 is straightforward. Observe that each non-transformed Reynolds number, effectively $R_k = 1/\mu^{[k]}$, is multiplied by the product of a sheared layer width and a plug velocity. Equally, each non-transformed Bingham number, $B_k = \tau_{\text{yield}}^{[k]}/\mu^{[k]}$, is multiplied by a sheared layer width and is divided by a plug velocity. Thus, provided that the plug velocities are smaller than the values that are found for the single fluid flows, increased stability will result. Note that, as the width of each sheared layer tends to zero, the corresponding plug velocity, which is proportional to the square of the width of the sheared fluid layer, tends to zero at a faster rate, and therefore $B \rightarrow \infty$. Thus, in the parameter space that we consider there is always an interval of Y_i for which improved stability is found.

To exploit the improved stability for stable transport of fluid 1 (i.e. via lubrication), we would require that the gain in stability is not offset too much by a reduction in flow rate of fluid 1. In Fig. 7c, we plot the (areal) flow rates through each fluid layer, $q_1(Y_i)$ and $q_2(Y_i)$:

$$q_1(Y_i) = \int_0^{Y_i} U(y) dy = 1 - q_2(Y_i). \quad (96)$$

It can be seen that in the interval of Y_i where stability is improved, $q_1(Y_i)$ is significantly reduced. Thus, $(\tau_{\text{yield}}^{[1]}, \tau_{\text{yield}}^{[2]}, \mu^{[1]}, \mu^{[2]}) = (0.1, 0.5, 0.01, 0.001)$ are not ideal parameters for the transport application. Since the total flow rate is always equal to unity, transport applications of the type described above will want to shift the interval of improved stability as close to the wall as possible. This implies a fluid 1 flow that is lubricated with a thin layer of fluid 2. To achieve thin layers with the double Bingham–Poiseuille profile requires that $Y_{i,\max} \leq Y_i \leq Y_{i,\min} \approx 1$. Parametrically, these flows are found close to the shaded region of Fig. 2. Fig. 8 shows analogous results to Fig. 7, but for rheological parameters $(\tau_{\text{yield}}^{[1]}, \tau_{\text{yield}}^{[2]}, \mu^{[1]}, \mu^{[2]}) = (0.002, 0.005, 0.0005, 0.0001)$, that lie closer to the shaded region of Fig. 2b. By comparison with Fig. 7, the change in fluid 1 Reynolds number for $Y_i \in [Y_{i,\min}, 1]$ is much reduced. Similarly, the region $Y_i \in [Y_{i,\min}, 1]$, in which $1/B$ decreases for fluid 1, is also reduced. The net effect therefore is to increase

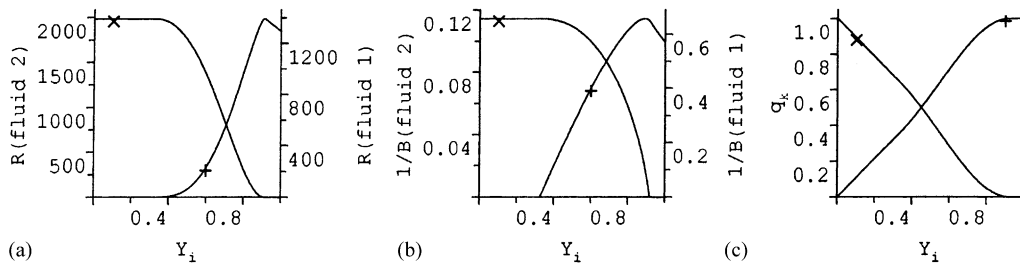


Fig. 8. Variations with Y_i : (a) R for each fluid, following the transformations of Section 4.3; (b) B for each fluid, following the transformations of Section 4.3; (c) q_1 and q_2 . Rheological parameters are $(\tau_{\text{yield}}^{[1]}, \tau_{\text{yield}}^{[2]}, \mu^{[1]}, \mu^{[2]}) = (0.002, 0.005, 0.0005, 0.0001)$. Fluid 1 marked with '+', fluid 2 marked with 'x'.

the interval of Y_i on which improved stability is found, to occupy most of the double Bingham–Poiseuille interval, $Y_i \in (Y_{i,\max}, Y_{i,\min})$. In the limit that $Y_{i,\min} \rightarrow 1$ the entire double Bingham–Poiseuille will have a reduced fluid 1 Reynolds number and increased Bingham number.

5.2. Visco-plastic lubricated transport of Newtonian fluids

We now consider the feasibility of using a visco-plastic fluid (fluid 2) to lubricate the transport of a Newtonian fluid. Note that the observed increased stability results from fluid 2 being unyielded at the interface. There is no necessity for fluid 1 to have a yield stress. For this section, we re-pose the problem in dimensional variables in order to ease application of the results. Dimensional variables will be denoted with the *hat* symbol, e.g. \hat{y} . Again, we assume symmetry of the flow about the centreline of the plane channel and only consider *half* the problem for simplicity.

Suppose that we wish to transport a given (areal) flow rate \hat{Q}_1 of fluid 1 through (half) a plane channel of (half-)width \hat{D} , the fluid having density $\hat{\rho}$ and viscosity $\hat{\mu}^{[1]}$. It is supposed that \hat{Q}_1 is such that the single fluid Reynolds number R (fluid 1):

$$R \text{ (fluid 1)} = \frac{3\hat{\rho}\hat{Q}_1}{2\hat{\mu}^{[1]}}$$

is in some sense *too large*, e.g. either transitional or fully turbulent, or even such that interfacial instabilities arise for conventional lubricants.

Our aim is to design a fluid 2 lubricant (i.e. choose the rheology of fluid 2), such that we can maintain the desired flow rate of fluid 1, \hat{Q}_1 , but reduce the Reynolds number in the fluid 1 layer. At the same time we require that the lubricating layer of fluid 2 remains stable. The example results in Figs. 7 and 8 suggest that lubrication will be most effective for a fluid rheology that allows $Y_{i,\min} \approx 1$. If the fluid 2 layer is unyielded, with interface at $\hat{y} = Y_i \hat{D}$, then fluid 1 adopts a plane Poiseuille flow profile in $\hat{y} \leq Y_i \hat{D}$ and the frictional pressure drop is given by

$$\left| \frac{d\hat{p}}{d\hat{x}} \right| = \frac{3\hat{Q}_1\hat{\mu}^{[1]}}{[Y_i\hat{D}]^3}.$$

Consequently, the fluid 2 yield stress is related to any chosen $Y_{i,\min}$ by

$$\hat{\tau}_{\text{yield}}^{[2]} = \frac{3\hat{Q}_1\hat{\mu}^{[1]}}{Y_{i,\min}^3 \hat{D}^2}. \quad (97)$$

Now, suppose a lubrication flow of fluid 2 that maintains the interface at $\hat{y} = Y_i \hat{D}$, with $Y_i \leq Y_{i,\min}$, whilst ensuring the flow rate \hat{Q}_1 of fluid 1. Assuming that fluid 2 does not yield at the interface, we have a Bingham–Poiseuille profile in the fluid 2 layer, with interfacial (plug) velocity $\hat{U}_{p,2}$ given by

$$\hat{U}_{p,2} = \frac{1}{2\hat{\mu}^{[2]}} \left| \frac{d\hat{p}}{d\hat{x}} \right| \hat{D}^2 (1 - Y_{\text{yield}}^{[2]})^2,$$

where $Y_{\text{yield}}^{[2]}$ is defined by

$$\left| \frac{d\hat{\rho}}{d\hat{x}} \right| = \frac{\hat{D}\hat{\tau}_{\text{yield}}^{[2]}}{Y_{\text{yield}}^{[2]}}. \quad (98)$$

The flow rate in the fluid 1 layer is given by

$$\hat{Q}_1 = \hat{D}Y_i\hat{U}_{p,2} + \left| \frac{d\hat{\rho}}{d\hat{x}} \right| \frac{[Y_i\hat{D}]^3}{3\hat{\mu}^{[1]}} = \hat{D}^3 \left| \frac{d\hat{\rho}}{d\hat{x}} \right| \left[\frac{Y_i^3}{3\hat{\mu}^{[1]}} + \frac{Y_i(1 - Y_{\text{yield}}^{[2]})^2}{2\hat{\mu}^{[2]}} \right], \quad (99)$$

which, after a little algebra, becomes an equation for $Y_{\text{yield}}^{[2]}$:

$$(Y_{\text{yield}}^{[2]})^2 - \left(2 + \frac{2}{3\varphi_\mu} \frac{Y_{i,\min}^3}{Y_i} \right) Y_{\text{yield}}^{[2]} + \left(1 + \frac{2}{3\varphi_\mu} Y_i^2 \right) = 0. \quad (100)$$

Recall that $\varphi_\mu \equiv \mu^{[1]}/\mu^{[2]} = \hat{\mu}^{[1]}/\hat{\mu}^{[2]}$. The relevant root is

$$Y_{\text{yield}}^{[2]} = \frac{2 + (2/3\varphi_\mu)(Y_{i,\min}^3/Y_i) - \sqrt{((2/3\varphi_\mu)(Y_{i,\min}^3/Y_i))^2 + (8/3\varphi_\mu)((Y_{i,\min}^3/Y_i) - Y_i^2)}}{2}, \quad (101)$$

and $|d\hat{\rho}/d\hat{x}|$ is then given by (98).

Supposing that $Y_{\text{yield}}^{[2]} > Y_i$ we can apply the transformations in Section 4.3 to each fluid layer. To do this we need to adopt the scaling used earlier in the paper. Note that the flow rate through the fluid 2 layer will be given by

$$\hat{Q}_2 = \hat{D}^3 \left| \frac{d\hat{\rho}}{d\hat{x}} \right| \frac{(1 - Y_{\text{yield}}^{[2]})^2(2 + Y_{\text{yield}}^{[2]} - 3Y_i)}{6\hat{\mu}^{[2]}}. \quad (102)$$

Thus, the total flow rate through half the slot is simply $\hat{Q}_1 + \hat{Q}_2$ and we can now define the mean velocity scale \hat{U}_0 straightforwardly:

$$\begin{aligned} \hat{U}_0 &= \frac{\hat{Q}_1 + \hat{Q}_2}{\hat{D}} = \hat{D}^2 \left| \frac{d\hat{\rho}}{d\hat{x}} \right| \left[\frac{(1 - Y_{\text{yield}}^{[2]})^2(2 + Y_{\text{yield}}^{[2]})}{6\hat{\mu}^{[2]}} + \frac{Y_i^3}{3\hat{\mu}^{[1]}} \right] \\ &= \frac{\hat{D}\hat{\tau}_{\text{yield}}^{[2]}}{\hat{\mu}^{[2]}} \frac{1}{Y_{\text{yield}}^{[2]}} \left[\frac{(1 - Y_{\text{yield}}^{[2]})^2(2 + Y_{\text{yield}}^{[2]})}{6} + \frac{Y_i^3}{3\varphi_\mu} \right]. \end{aligned} \quad (103)$$

We scale all velocities with \hat{U}_0 , the yield stresses are scaled with $\hat{\rho}\hat{U}_0^2$, viscosities are scaled with $\hat{\rho}\hat{U}_0\hat{D}$, and lengths are scaled with \hat{D} . Having done this we apply the transformations in Section 4.3 to all scaled rheological variables and *plug* velocities. We spare the reader the algebraic details.

The transformed Reynolds number for the fluid 1 layer is given by

$$R(\text{fluid 1}) = \frac{\hat{\rho}\hat{D}^2\hat{\tau}_{\text{yield}}^{[2]} Y_i^3}{(\hat{\mu}^{[1]})^2 2Y_{\text{yield}}^{[2]}}, \quad (104)$$

whereas for the flow of fluid 1 alone, we have

$$R(\text{fluid 1}) = \frac{\hat{\rho} \hat{D}^2 \hat{\tau}_{\text{yield}}^{[2]} Y_{i,\min}^3}{(\hat{\mu}^{[1]})^2} \frac{1}{2}. \quad (105)$$

Therefore, the lubricating layer serves to reduce the fluid 1 Reynolds number by a factor of: $Y_i^3 / (Y_{i,\min}^3 Y_{\text{yield}}^{[2]})$.

In the lubricating fluid 2 layer we find that

$$R(\text{fluid 2}) = \frac{\hat{\rho} \hat{D}^2 \hat{\tau}_{\text{yield}}^{[2]} (1 - Y_{\text{yield}}^{[2]})^3}{(\hat{\mu}^{[2]})^2} \frac{1}{2 Y_{\text{yield}}^{[2]}} = \frac{\hat{\rho} \hat{D}^2 \hat{\tau}_{\text{yield}}^{[2]} Y_{i,\min}^3 \varphi_\mu^2 (1 - Y_{\text{yield}}^{[2]})^3}{2(\hat{\mu}^{[1]})^2 Y_{i,\min}^3 Y_{\text{yield}}^{[2]}}, \quad (106)$$

and

$$B(\text{fluid 2}) = \frac{2 Y_{\text{yield}}^{[2]}}{(1 - Y_{\text{yield}}^{[2]})}. \quad (107)$$

Note that since for the single fluid flow of fluid 1, $R(\text{fluid 1}) = (\hat{\rho} \hat{D}^2 \hat{\tau}_{\text{yield}}^{[2]} Y_{i,\min}^3) / (2(\hat{\mu}^{[1]})^2)$, the quantity $[\varphi_\mu^2 (1 - Y_{\text{yield}}^{[2]})^3] / [Y_{i,\min}^3 Y_{\text{yield}}^{[2]}]$ gives an indication of how large the fluid 2 Reynolds number will be in comparison to the original fluid 1 Reynolds number.

5.2.1. Application

To use the above analysis to design a suitable visco-plastic lubricating fluid, the following requirements should be satisfied:

1. Keep $Y_{\text{yield}}^{[2]} \approx Y_{i,\min} \approx 1$, i.e. a thin sheared layer of the lubricating fluid.
2. Select the plastic viscosity of fluid 2 to ensure $\varphi_\mu \gg 1$. This is inevitable if we are trying to exploit fluid 2 as a lubricant.
3. Make $Y_i^3 / (Y_{i,\min}^3 Y_{\text{yield}}^{[2]})$ as small as is possible (this parameter defines is the reduction in the fluid 1 Reynolds number, over the single fluid value).
4. Keep $[\varphi_\mu^2 (1 - Y_{\text{yield}}^{[2]})^3] / [Y_{i,\min}^3 Y_{\text{yield}}^{[2]}] \sim 1$, and rely on the increase in $B(\text{fluid 2}) = 2 Y_{\text{yield}}^{[2]} / (1 - Y_{\text{yield}}^{[2]})$, to maintain stability in the lubricating layer.

There is some conflict between requirements (2) and (4) above, so a compromise needs to be attained. However, we demonstrate below that a significant reduction in fluid 1 Reynolds number is feasible.

We select $Y_{i,\min} = 0.95$ and consider the above requirements. First of all, its clear that to satisfy (4) we must balance φ_μ^2 with $(1 - Y_{\text{yield}}^{[2]})^3$. However, it is less clear that $(1 - Y_{\text{yield}}^{[2]})$ will remain small if Y_i is not close to $Y_{i,\min}$. In Fig. 9a, we plot $(1 - Y_{\text{yield}}^{[2]})$ and show that this is indeed the case. In Fig. 9b, we plot the quantity $Y_i^3 / (Y_{i,\min}^3 Y_{\text{yield}}^{[2]})$ with contour levels 0.05. Each contour level represents a 5% reduction in the Reynolds number of the fluid 1 layer and the shaded region represents reductions between 50 and 100% of the single fluid value. Comparing with Fig. 9a it is clear that a significant reduction in Reynolds number is possible, whilst maintaining $(1 - Y_{\text{yield}}^{[2]})$ small.

Now, we turn to the fluid 2 lubricating layer. Fig. 9c shows the contours of the quantity $[\varphi_\mu^2 (1 - Y_2)^3] / [Y_{i,\min}^3 Y_{\text{yield}}^{[2]}]$, plotted at intervals 1. The shaded region shows where the Reynolds number of the fluid 2 layer will be lower than that of the single fluid flow of fluid 1. Fig. 9d shows the variation in $1/B(\text{fluid 2})$

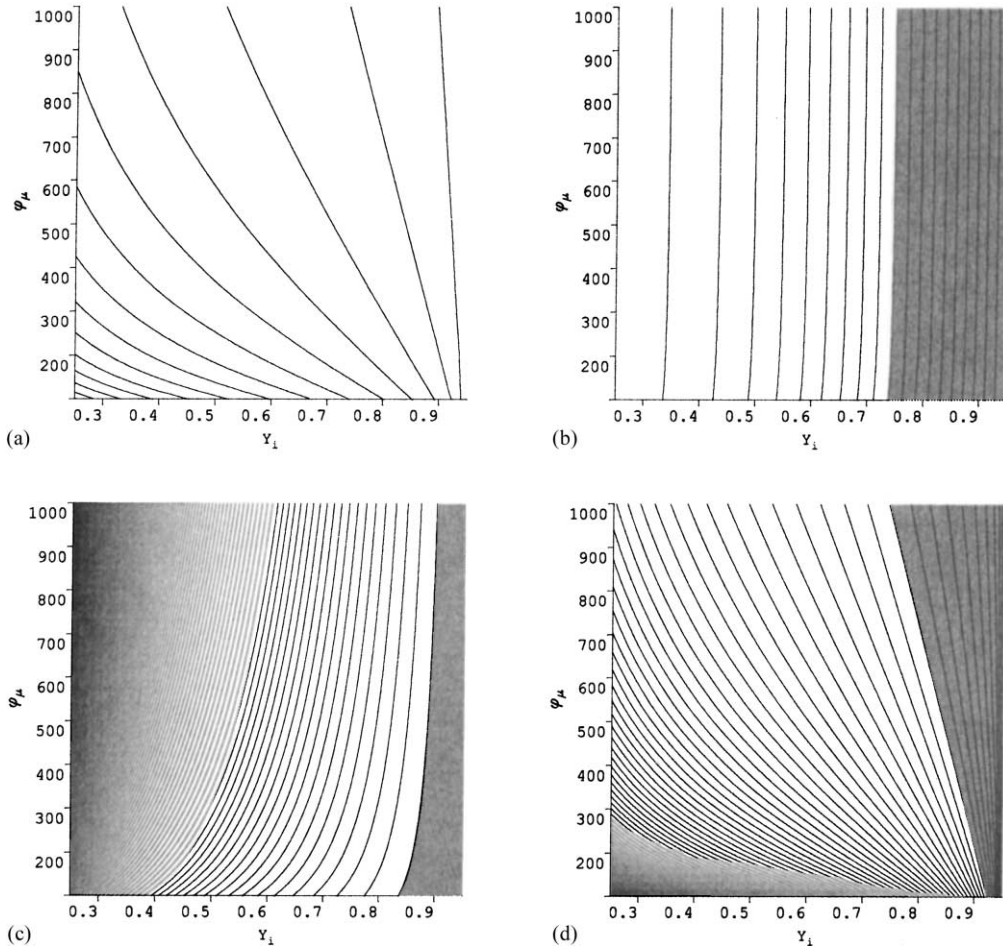


Fig. 9. Variations in various quantities with (Y_i, φ_μ) : (a) $1 - Y_{\text{yield}}^{[2]}$, contours intervals 0.01; (b) $Y_i^3 / (Y_{i,\text{min}}^3 Y_{\text{yield}}^{[2]})$ (reduction in the fluid 1 Reynolds number), contour intervals 0.05; the shaded region denotes reductions of 50–100%; (c) $[\varphi_\mu^2 (1 - Y_2)^3] / [Y_{i,\text{min}}^3 Y_{\text{yield}}^{[2]}]$ contour intervals 1; the shaded area denotes where the fluid 2 Reynolds number is less than the single fluid Reynolds number for fluid 1; (d) $1/B$ (fluid 2), contour intervals 10^{-3} the shaded region denotes where B (fluid 2) > 100 .

over the same range of (Y_i, φ_μ) . Contours plotted are at intervals 10^{-3} and the shaded region in Fig. 9c has a Bingham number in excess of 10^2 .

In order to make laminar a Newtonian flow that is approximately transitional, we would need to select a lubricant and interface position in the upper right corner of Fig. 9. By remaining in the shaded areas of Fig. 9c and d, we ensure that the fluid 2 Reynolds number is less than the original fluid 1 Reynolds number. The increase in Bingham number ensures linear stability of the lubricating layer. By moving away from the upper right corner of Fig. 9, we reduce the effective Reynolds number of fluid 1. Thus, a reduction of 25% appears easily attainable.

If the Newtonian flow is not transitional, but we would like to transport the fluid at a flow rate corresponding say to a single fluid Reynolds number of order 100, then we might allow a fluid 2 Reynolds

number of order 1000, without shear instabilities arising in the lubricating layer. Thus, in Fig. 9c we can operate about 10 contour levels outside of the shaded region. Moving 10 contours outside of the shaded region in Fig. 9d still gives Bingham numbers over 50. It is evident that there is a large overlap between Fig. 9c and d, and thus in Fig. 9b we can select m (0.65, 500) and reduce the fluid 1 Reynolds number to 30% of its original value.

As an example, suppose we would like to lubricate the passage of a viscous liquid with $\hat{\mu}^{[1]} = 0.1$ Pa s, $\hat{\rho} = 1500$ kg/m³, at 0.5 m/s through a channel with $\hat{D} = 0.05$ m. Thus, $\hat{Q}_1 = 0.025$ m²/s and the single fluid Reynolds number is R (fluid 1) = 562.5. At such a large Reynolds number, most multi-layer flows will suffer from interfacial instabilities. We match the density of our lubricant, select $Y_{i,\min} = 0.95$, which gives $\hat{\tau}_{\text{yield}}^{[2]} = 3.499$ Pa. Now by selecting $\hat{\mu}^{[2]} = 0.0002$ Pa s we have $\varphi_{\mu} = 500$ and in a multi-layer flow with interface at $Y_i \approx 0.8$ the fluid 1 Reynolds number is reduced to approximately 330 while the fluid 2 Reynolds number is approximately 1600 with a Bingham number ≈ 75 .

6. Summary and discussion

The key result of this paper is that parallel multi-layer flows of two Bingham fluids, for which an unyielded plug region is adjacent to the interface, will not suffer from the classical linear interfacial instabilities that are found for analogous multi-layer flows of Newtonian and many other non-Newtonian fluids. Instead, such flows first become linearly unstable to shear instabilities that are analogous to those found for single fluid flows. Linear shear instabilities arise generally at Reynolds numbers $\sim 10^3$, whereas the linear interfacial instabilities that result from using classical fluids for multi-layer fluid lubrication, arise either unconditionally, or for Reynolds numbers 1–10 (typically with complex marginal stability criteria). Therefore, it may be possible to observe stable *visco-plastically* lubricated flows at relatively high speeds.

In Section 5.2, we have shown that this is indeed feasible for the lubricated transport of Newtonian fluids, at least from the point of view of maintaining linear stability. Since interfacial instabilities are often a key factor that limit production rates in industrial processes that involve multi-layer flows, the use of visco-plastic fluids as lubricants has significant industrial potential. The physical benefits of such usage would seem to fall into one of three categories:

1. To use as a lubricant that does not suffer from linear interfacial instability.
2. To use in place of a lubricant that would suffer from interfacial instability at a given flow rate (i.e. moderate Reynolds numbers).
3. To use as a lubricant at high flow rates, where the single fluid flow would be turbulent (flow laminarisation).

To balance the above optimism, we note the following.

- Visco-plastic lubrication flows of the type analysed require a larger pressure drop than the associated single fluid non-lubricated flow. Thus, usage for large-scale pipelining applications (e.g. coal–water slurry transport and oil–water transport), is probably not practical.
- The laminarisation application in Section 5.2 results in lubricant flows for which the yielded lubricant layers are relatively thin. This type of flow may be hard to establish and control in a large-scale hydraulics application.

With a view to the above points, likely areas for application are small-scale co-extrusion processes where surface or interfacial quality is paramount and where accurate flow control can be realised. We have not sought a direct process application. The aim of the paper has been simply to show feasibility of the method and the exciting possibilities that exist for a visco-plastic lubricant. Application would require physico-chemical design of a suitable lubricant system for which a range of different rheologies can be achieved, focused at a specific process application. This lies far outside of the expertise of the author.

In a sense the results are quite general. The same analysis of the interface is true for any other inelastic yield-stress fluid (e.g. Herschel–Bulkley, Casson, etc.), for which the unyielded plug is not perturbed by a linear perturbation with zero mean. Although we would need to repeat the analysis in the appendix for each fluid, the underlying physical principal is that an infinitely long *solid* plug region cannot be accelerated by an infinitesimal perturbation which exerts no net traction. This appears to be a sensible statement, independent of fluid type. We therefore expect similar stability results for these other fluid types. Here we have considered only plane Poiseuille flows. However, the same interfacial analysis will be true for other multi-layer flows of visco-plastic fluids which maintain an unyielded plug region at the interface(s) for the basic flow. Thus, mixed Couette–Poiseuille and other practical basic flows may also exist with enhanced linear stability characteristics and the same analysis can be widely applied to other practical duct flows, particularly pipe flows.

If we examine carefully the analysis carried out in the paper, it is seen that the reason for the elimination of interfacial instabilities rests with motion of the plug region. In a multi-layer parallel Newtonian flow, we have the interfacial condition

$$y_i(x, t)U'(Y_i^+) + u(x, Y_i^+, t) = y_i(x, t)U'(Y_i^-) + u(x, Y_i^-, t), \quad (108)$$

for linear perturbations y_i and u . Because the shear stress is conserved at the interface, a jump in U' results and there is a non-zero jump in the perturbed axial velocity. For the visco-plastic lubricant, the above condition becomes

$$u(x, Y_i^+, t) = y_i(x, t)U'(Y_i^-) + u(x, Y_i^-, t), \quad (109)$$

since the plug region is unyielded. The analysis of the plug motion then gives that $v_p^{[2]} = 0$ for normal modes with non-zero wave-number and the kinematic condition implies that $y_i = 0$ for such normal modes. Thus, in effect we have the simple continuity condition

$$u(x, Y_i^+, t) = u(x, Y_i^-, t), \quad (110)$$

at the interface for the visco-plastic lubricant. Although the transformations in Section 4.3 are an elegant method of problem simplification, it is really the above conditions that allow the linear stability problems in the two unyielded fluid regions to be effectively uncoupled.

An obvious restriction to the analysis in this paper is that we have considered only a linear stability analysis. A key practical question is whether or not the same flows are non-linearly stable, to small finite perturbations, and indeed whether or not these flows can be observed experimentally. In [18] we have recently considered the nonlinear stability of Poiseuille flows of Bingham fluids. The same methods seem to have potential here, but the analysis is fairly complex.

As for direct experimental validation of our results, we know the known experimental results. Recent experiments by Gabard [19], are interesting in the context of this paper and discussion. Gabard displaces aqueous solutions of both Xanthan and Carbopol with a less viscous glycerol solution along a long

(non-capillary) tube. The Xanthan solutions are Carreau-like with a very large low shear viscosity, whereas the Carbopol solutions exhibit a yield stress, (approximately Herschel-Bulkley). The flow rates and glycerol viscosity are such that the displacement is incomplete. A thick uniform layer of fluid 2 is left behind on the walls of the tube directly following the initial displacement in each case. In the context of this paper, well behind the displacement front, the axial velocity profiles for the Carbopol solutions are of the static wall layer type, (see Fig. 4c). The wall layer for the Xanthan solutions is pseudo-static, i.e. moving imperceptibly. The glycerol solution is pumped past the wall layers for some time after the displacement front has passed. The Xanthan solutions were observed to become slowly unstable, whereas the Carbopol solutions (with a true yield stress) were not observed to become unstable. These results lend some credence to the results derived here, even if only the static wall layer regime is addressed. Ideally we would like to run a set of experiments targeted specifically at the mobile visco-plastic lubrication flows analysed here.

As a final comment, note that in our results it is critically necessary that the fluids used as lubricants have a true yield stress at zero shear. The results in [12] indicate that the enhanced linear stability will be lost if the fluids have only an apparent yield stress. Since regularised viscosity models are commonly used for modelling yield stress fluids these results are very interesting. The regularised viscosity models can be viewed as a perturbation of the true Bingham fluid constitutive equations. The results in this paper suggest that such a perturbation can be singular, at least as far as equations of hydrodynamic stability are concerned.

References

- [1] C.-S. Yih, Instability due to viscosity stratification, *J. Fluid Mech.* 27 (2) (1967) 337–352.
- [2] C.E. Hickox, Instability due to viscosity and density stratification in axisymmetric pipe flow, *Phys. Fluids* 14 (2) (1971) 251–262.
- [3] A.P. Hooper, W.G. Boyd, Shear flow instability due to a wall and a viscosity discontinuity at the interface, *J. Fluid Mech.* 179 (1987) 201–225.
- [4] S.G. Yiantsos, B.G. Higgins, Linear stability of plane Poiseuille flow of two superposed fluids, *Phys. Fluids* 31 (1988) 3225–3238.
- [5] D.D. Joseph, Y.Y. Renardy, *Fundamentals of Two-Fluid Dynamics*. Interdisciplinary Applied Mathematics, Springer, 1993.
- [6] E.J. Hinch, A note on the mechanism of the instability at the interface between two shearing fluids, *J. Fluid Mech.* 114 (1984) 463–465.
- [7] F. Charru, Phase diagram of interfacial instabilities in two-layer shear flows, in: *Proceedings of the Third International Conference on Multiphase Flow, ICMF'98, Lyon, France, 8–12 June 1998*.
- [8] N.D. Waters, The stability of two stratified power law fluids in Couette flow, *J. Non-Newt. Fluid Mech.* 12 (1983) 85–94.
- [9] N.D. Waters, A.M. Keeley, The stability of two stratified non-Newtonian liquids in Couette flow, *J. Non-Newt. Fluid Mech.* 24 (1987) 161–181.
- [10] B. Khomami, Interfacial stability and deformation of two stratified power law fluids in plane Poiseuille flow, part 1. stability analysis, *J. Non-Newt. Fluid Mech.* 36 (1990) 289–303.
- [11] Y.Y. Su, B. Khomami, Stability of multi-layer power law and second order fluids in plane Poiseuille flow, *Chem. Eng. Commun.* 109 (1991) 209–223.
- [12] A. Pinarbasi, A. Liakopoulos, Stability of two-layer Poiseuille flow of Carreau-Yasuda and Bingham-like fluids, *J. Non-Newt. Fluid Mech.* 57 (1995) 227–241.
- [13] M. Allouche, I.A. Frigaard, G. Sona, Static wall layers in the displacement of two visco-plastic fluids in a plane channel, *J. Fluid Mech.* 424 (2000) 243–277.
- [14] I.A. Frigaard, O. Scherzer, G. Sona, Uniqueness and non-uniqueness in the steady displacement of two viscoplastic fluids, *ZAMM* 81 (2) (2001) 99–118.

- [15] I.A. Frigaard, S.D. Howison, I.J. Sobey, On the stability of Poiseuille flow of a Bingham fluid, *J. Fluid Mech.* 263 (1994) 133–150.
- [16] E. Comparini, P. Mannucci, Flow of a Bingham fluid in contact with a Newtonian fluid, *J. Math. Anal. Appl.* 227 (1998) 359–381.
- [17] I.A. Frigaard, O. Scherzer, Uniaxial exchange flows of two Bingham fluids in a cylindrical duct, *IMA J. Appl. Math.* 61 (1998) 237–266.
- [18] C. Nouar, I.A. Frigaard, Nonlinear stability of Poiseuille flow of a Bingham fluid theoretical results and comparison with phenomenological criteria, *J. Non-Newtonian Fluid Mech.* (2001), submitted for publication.
- [19] C. Gabard, Etude de la stabilité de films liquides sur les parois d'une conduite verticale lors de l'écoulement de fluides miscibles non-newtoniens. These de l'Universite Pierre et Marie Curie, Ph.D. Thesis, Orsay, France, 2001.